Functional alterations in cortical processing of speech in glioma-infiltrated cortex

Alexander A. Aabedi[a,1], Benjamin Lipkin[b,1], Jasleen Kaur[a], Sofia Kakaizada[a], Claudia Valdivia[a], Sheantel Reihl[a], Jacob S. Young[a], Anthony T. Lee[a], Saritha Krishna[a], Mitchel S. Berger[a], Edward F. Chang[a], David Brang[b,2], and Shawn L. Hervey-Jumper[a,2]

[a]Department of Neurological Surgery, University of California, San Francisco, CA, 94143; and [b]Department of Psychology, University of Michigan, Ann Arbor, MI, 48109

Edited by Patricia K. Kuhl, University of Washington, Seattle, WA, and approved October 8, 2021 (received for review May 14, 2021)

Recent developments in the biology of malignant gliomas have demonstrated that glioma cells interact with neurons through both paracrine signaling and electrochemical synapses. Glioma–neuron interactions consequently modulate the excitability of local neuronal circuits, and it is unclear the extent to which glioma-infiltrated cortex can meaningfully participate in neural computations. For example, gliomas may result in a local disorganization of activity that impedes the transient synchronization of neural oscillations. Alternatively, glioma-infiltrated cortex may retain the ability to engage in synchronized activity in a manner similar to normal-appearing cortex but exhibit other altered spatiotemporal patterns of activity with subsequent impact on cognitive processing. Here, we use subdural electrocorticography to sample both normal-appearing and glioma-infiltrated cortex during speech. We find that glioma-infiltrated cortex engages in synchronous activity during task performance in a manner similar to normal-appearing cortex but recruits a diffuse spatial network. On a temporal scale, we show that signals from glioma-infiltrated cortex have decreased entropy, which may affect its ability to encode information during nuanced tasks such as production of monosyllabic versus polysyllabic words. Furthermore, we show that temporal decoding strategies for distinguishing monosyllabic from polysyllabic words were feasible for signals arising from normal-appearing cortex but not from glioma-infiltrated cortex. These findings inform our understanding of cognitive processing in chronic disease states and have implications for neuromodulation and prosthetics in patients with malignant gliomas.

glioma | neural circuitry | speech | glioma electrophysiology | neural decoding

Gliomas are the most common intrinsic brain tumors and a leading cause of neurological impairment in adults. Mounting evidence suggests that malignant gliomas remodel functional neuronal networks and that these cellular- and network-level interactions impact cognition and survival (1). The mechanistic underpinnings of glioma–neuron interactions and their influence on human cognition is incompletely understood. Recent studies have shown that gliomas not only interact with neurons through paracrine signaling but also through de novo electrophysiologically coupled synapses. As such, glioma-infiltrated cortex maintains activity-dependent connections to disparate brain regions (2–4). These findings challenge the notion that infiltrative gliomas simply lead to the destruction and loss of function within tumor-infiltrated brain regions, raising instead the possibility that brain cancer may fundamentally alter the way infiltrated brain regions perform the computations required for cognition and behavior.

There are two primary means by which gliomas may alter the electrophysiology of the human cortex. On one hand, glioma invasion may lead to locally disorganized activity that impedes the transient synchronization of neural oscillations required for the binding of task-relevant information (5). If this were the case, glioma-infiltrated cortex would not meaningfully participate in neural computations. Alternatively, glioma-infiltrated cortex may retain the ability to engage in synchronized activity in a manner similar to normal-appearing cortex but suffer from a degradation in the amount and quality of information encoded on a temporal scale. The effects of glioma infiltration on the spatial recruitment of language areas during speech similarly remain unclear. If computations are indeed fully disrupted, cortical recruitment may be limited. However, if synchronous function is instead preserved, it may be possible to observe widespread activity in glioma-infiltrated regions.

The extent to which information is processed within tumor-infiltrated cortex in the human brain is unknown. A better understanding of the biology of speech within glioma-infiltrated cortex will add to our understanding of language processing and facilitate the development of electrophysiologically based interventions (i.e., neuroprosthetics and neuromodulation) for the restoration and rehabilitation of neurological function (6). Here, we test the hypothesis that glioma-infiltrated cortex retains event-related neuronal synchrony with an altered capacity for information encoding compared to normal-appearing cortex. To do so, we acquired invasive electrophysiologic

Significance

As gliomas proliferate, they infiltrate healthy brain tissue. Often, patients with such tumors in the language areas of the brain develop aphasia. Understanding how gliomas interact with normal neural circuits is critical for developing neuroprostheses that restore speech. Recent evidence demonstrates that glioma cells interact synaptically with neurons and thus can modulate neural circuits. However, it is unclear the extent to which glioma-infiltrated cortex participates in cognitive processing. Using electrocorticography to record both glioma-infiltrated and normal-appearing cortex during speech, we found that glioma-infiltrated cortex is capable of coordinated neural responses but has reduced capacity for information encoding. Instead, glioma-infiltrated cortex recruits a broader network of cortical regions during speech, which may represent a compensatory mechanism with implications for future neuroprostheses.

Author contributions: J.S.Y., A.T.L., S. Krishna, M.S.B., E.F.C., D.B., and S.L.H.-J. designed research; A.A.A., B.L., J.K., S. Kakaizada, D.B., and S.L.H.-J. performed research; A.A.A. contributed new reagents/analytic tools; A.A.A., B.L., C.V., S.R., D.B., and S.L.H.-J. analyzed data; and A.A.A., B.L., and S.L.H.-J. wrote the paper.

The authors declare no competing interest.

This article is a PNAS Direct Submission.

[1]A.A.A. and B.L. contributed equally to this work.

[2]To whom correspondence may be addressed. Email: shawn.hervey-jumper@ucsf.edu or djbrang@umich.edu.

This article contains supporting information online at http://www.pnas.org/lookup/suppl/doi:10.1073/pnas.2108959118/-/DCSupplemental.

Published November 9, 2021.

recordings (electrocorticography [ECoG]) in nonaphasic study participants with dominant hemisphere perisylvian malignant gliomas during speech production and spatially matched cortical sites for normal-appearing and glioma-infiltrated regions. We used Shannon entropy as a statistical proxy for the maximum encoding capacity of signals arising from glioma-infiltrated cortex. We then applied several distinct decoding paradigms to determine whether nuanced aspects of speech processing take place in glioma-infiltrated cortex (7).

Results

Our goal was to examine the computational capacity and decodability of neural signals arising from normal-appearing and glioma-infiltrated cortex during speech production from nonaphasic human study participants. As such, we recorded ECoG activity in 12 nonaphasic patients with malignant gliomas on the surface of the brain in language regions during a visual confrontation naming task (Fig. 1). Recordings were taken from participants with low-grade and high-grade gliomas (*SI Appendix*, Table S1) based on prior work demonstrating that they can form functional synaptic connections with neurons (2, 8–10) and induce circuit-level hyper-excitability, which may alter cortical processing (1, 11, 12). Oligodendrogliomas, astrocytomas, and glioblastomas were included. Because isocitrate dehydrogenase (IDH) mutant 1p/19 codeleted oligodendrogliomas may rely on distinct mechanisms to infiltrate the parenchyma and modulate cortical dynamics (11, 13), we performed additional analyses in a subgroup of noncodeleted gliomas (i.e., astrocytomas and glioblastomas IDH-wild type) and directly compared these results with the 1p/19q codeleted oligodendrogliomas.

In each participant, we first established the hemisphere of language dominance noninvasively using magnetic source imaging (14, 15). We then implanted subdural ECoG grids over the dominant perisylvian cortex, which was on the left side in all 12 participants. We used a combination of stereotactic neuronavigation and offline electrode registration methods to identify electrodes overlying regions of apparently normal parenchyma (i.e., devoid of T2-FLAIR signal abnormality; "normal-appearing") and regions with glioma invasion (i.e., within T2-FLAIR signal abnormality but outside the tumor core; "glioma-infiltrated") (*SI Appendix*, Fig. S1) (11).

Accordingly, we were able to sample from spatially matched regions and obtain excellent coverage of areas involved in the planning and articulation of speech (left inferior frontal gyrus and lateral precentral gyrus, respectively) (16) (Fig. 2 *A*–*D* and *SI Appendix*, Fig. S2). We then proceeded with our testing paradigm, which consisted of 48 unique visual stimuli depicting common objects or animals. Participants were required to name each item aloud while they underwent simultaneous audio and ECoG recordings.

Glioma-Infiltrated Cortex Engages in Coordinated Neural Responses during Speech. We extracted event-related spectral power perturbations (ERSPs) in the high-gamma range (70 to 170 Hz). During the production of speech, we found robust and coordinated responses in both normal-appearing and glioma-infiltrated cortex (Fig. 3*A*). This includes activation anterior to primary motor cortex beginning 800 ms prior to speech onset with maximal activity at the beginning of speech production (time = 0) (17). We then projected these responses onto a common cortical surface separately for normal-appearing and glioma-infiltrated cortex to examine the spatial involvement of the lateral prefrontal areas (Fig. 3*B*). In normal-appearing cortex, we observed maximal high-gamma activity in a spatially restricted region involving the canonical speech planning areas (pars orbitalis and triangularis of the inferior frontal gyrus) (18). By contrast, in glioma-infiltrated cortex, the spatial pattern of maximal high-gamma activity included not only the rostral inferior frontal gyrus but also diffuse areas of the middle frontal gyrus. These data suggest physiologically intact temporal patterns of neural responses in glioma-infiltrated cortex with broad spatial representations.

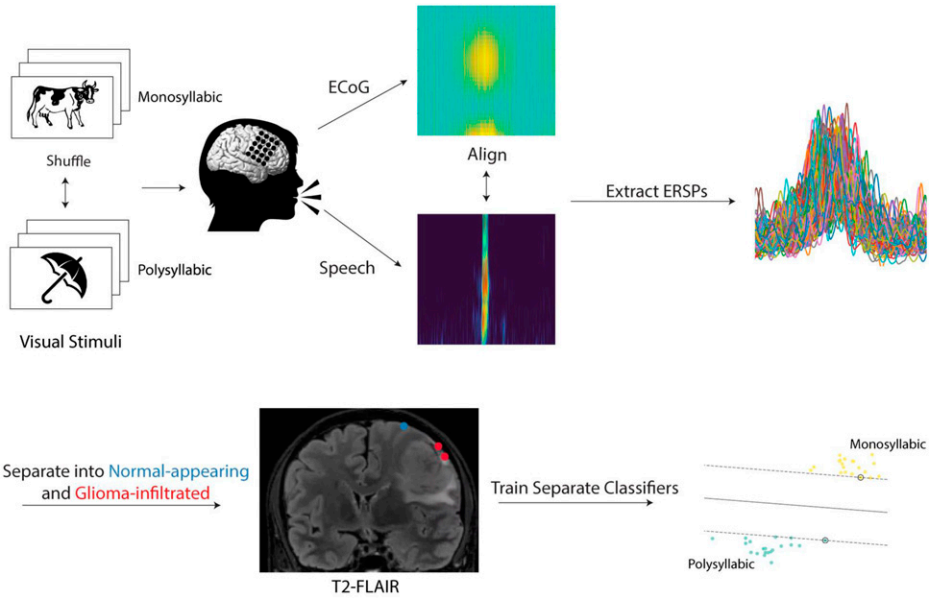

Fig. 1. Experimental workflow. Participants with perisylvian gliomas on the surface of the brain were asked to complete a picture naming task during intraoperative functional mapping. On each trial, participants were presented with a line drawing of a common object or animal in a randomized fashion and prompted to provide its name. Of the 48 stimuli, 28 represented monosyllabic words while 20 represented polysyllabic words. Audio and electrophysiologic (via ECoG) recordings were taken from each participant during task completion and aligned to speech onset. ERSPs were extracted in the high-gamma range (70 to 170 Hz). Electrodes were localized on each participant's preoperative T2-FLAIR image and categorized as "normal-appearing" if overlying normal-appearing cortex or "glioma-infiltrated" if overlying regions of T2-FLAIR signal abnormality. Using the ERSPs, separate classifiers were trained to decode the trial condition (monosyllabic versus polysyllabic) in normal-appearing and tumor-infiltrated cortex.

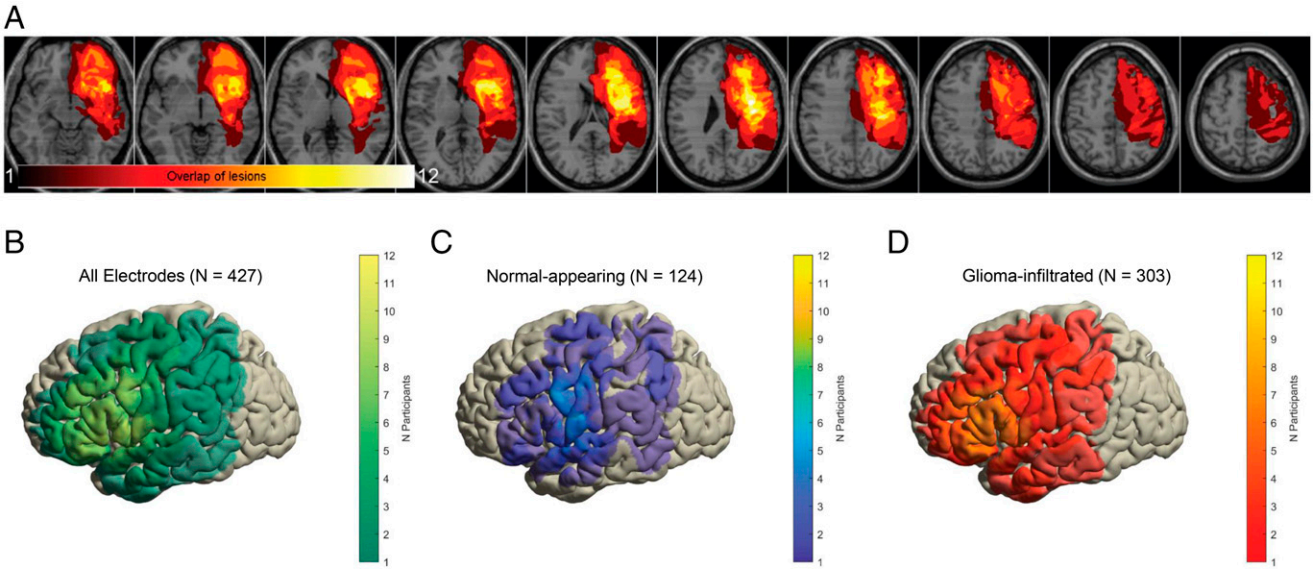

Fig. 2. Heatmaps demonstrating regions of glioma infiltration (*A*) and electrode coverage (*B–D*). (*A*) For each participant, regions of abnormally elevated T2-FLAIR signal representing glioma infiltration were manually segmented and interpolated in three dimensions. These segments were subsequently summed across all participants to generate a heatmap which demonstrates focal involvement of the left perisylvian language areas. (*B–D*) Common cortical surfaces showing the number of participants with electrode coverage at a given region: all electrodes (*B*), electrodes overlying normal-appearing cortex (*C*), and electrodes overlying glioma-infiltrated cortex (*D*). Speech planning and initiation sites are represented in both normal-appearing and glioma-infiltrated cortex.

We next determined whether regions of glioma-infiltrated cortex are functionally integrated with language networks. To do so, we performed cortical language mapping in all 12 participants using direct electrical stimulation, which is considered the clinical gold standard for the identification of functional cortex (19, 20). A given site was deemed as "positive" if its stimulation

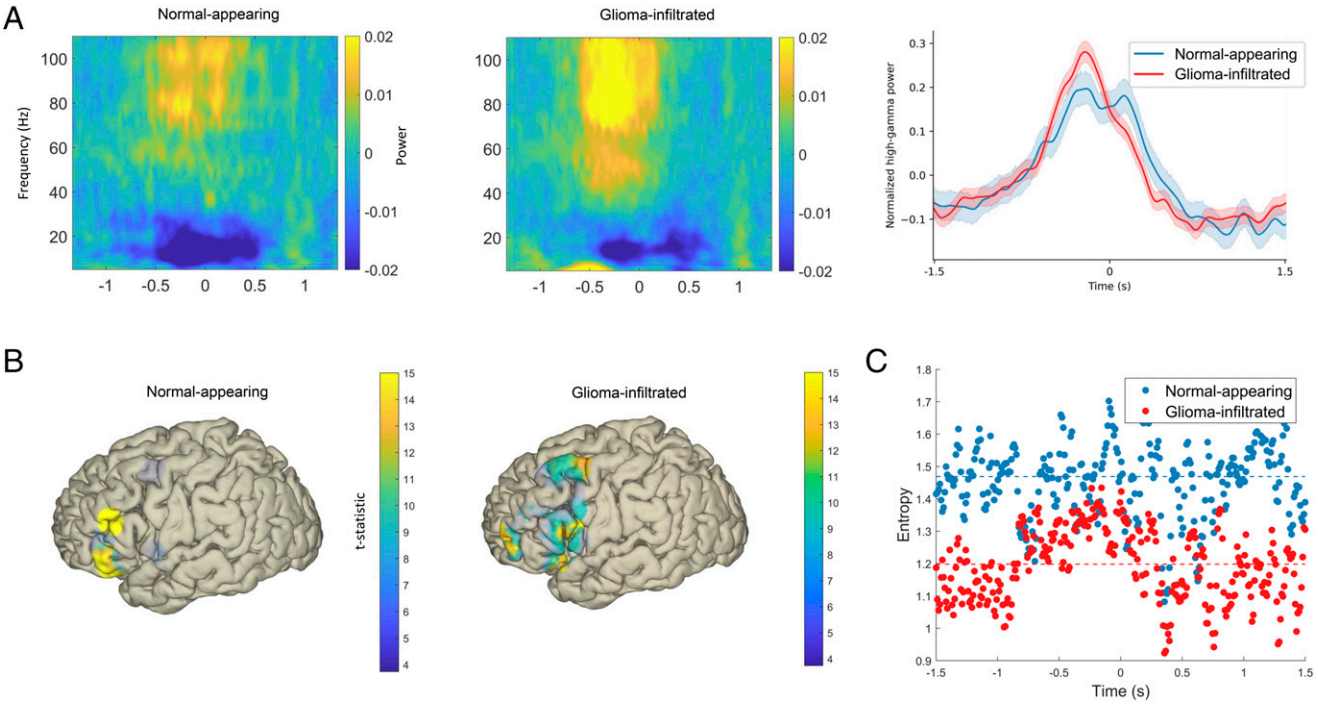

Fig. 3. Spatiotemporal features of neural signals from normal-appearing and glioma-infiltrated cortex during speech. (*A*) Broadband ERSPs in normal-appearing and glioma-infiltrated cortex (*Left* and *Middle*, respectively). (*Right*) ERSPs averaged over the high-gamma range with time = 0 representing speech onset (shading represents 95% confidence intervals). Both normal-appearing and glioma-infiltrated cortex demonstrate robust and coordinated increases in time-locked high-gamma activity. (*B*) Spatial representations of mean high-gamma activity during prespeech planning (−1,000 to 0 ms) relative to a postspeech baseline thresholded to a Bonferroni-corrected $P < 0.01$. In normal-appearing cortex (*Left*), activity is primarily restricted to the canonical speech planning sites, while activity is more diffuse in glioma-infiltrated cortex (*Right*). (*C*) The entropy at each time point in normal-appearing and glioma-infiltrated cortex. Signals from glioma-infiltrated cortex have lower entropy, a statistical proxy for information-encoding capacity ($P = 0.006$). Dashed lines represent sample medians.

led to anomia, semantic paraphasia, phonological paraphasia, neologisms, or circumlocution in two out of three stimulation trials during a picture naming task. In total, we found 19 positive language sites in our 12 participants (*SI Appendix*, Fig. S3). Of those 19 sites, 12 (63%) were in regions of glioma-infiltrated cortex, while 7 were in normal-appearing cortex. Together, these results demonstrate that glioma-infiltrated cortex engages in coordinated neural responses during speech production and that select regions remain functionally integrated within long-range functional circuits.

Signals from Glioma-Infiltrated Cortex Have Decreased Entropy. Having established that glioma-infiltrated cortex retains the ability to engage in coordinated neural responses and recruits a diffuse network of lateral prefrontal areas during speech production, we next set out to determine the relative capacity of these cortical regions to encode information. Therefore, in this setting, information was represented as mean high-gamma activity over time within glioma-infiltrated and normal-appearing cortex. Shannon's metric for information (entropy) provided a statistical proxy for the theoretical maximum of the signal's encoding capacity (21). We measured the entropy of neural signals at a) each time point in the event-related response to generate a time-course of entropy values (Fig. 3*C*) as well as b) averaged across all trials to derive a mean estimate (*SI Appendix*, Fig. S4). Using linear mixed-effects modeling to account for the hierarchical nature of the data, we found that glioma-infiltrated cortex had lower entropy and, therefore, a potentially lower capacity to encode information over time ($P < 0.0001$). Critically, the discrepancy in entropy was observed in regions of the brain required for speech production (*SI Appendix*, Fig. S4, *Right*). Lower entropies were observed in glioma-infiltrated cortex even when accounting for 1p/19q codeletion status ($P < 0.0001$). Overall entropy did not significantly vary across codeleted and noncodeleted participants ($P = 0.437$).

Neural Signals from Normal-Appearing but Not Glioma-Infiltrated Cortex Can Be Decoded. Given the coordinated neural responses yet diminished entropy of glioma-infiltrated cortex, we next set out to determine whether there are alterations in the high-gamma activity elicited by computationally demanding tasks. Vocalization of polysyllabic words, for instance, requires a more intricate coordination of articulatory elements than that of monosyllabic words. The reliability of sublexical articulatory encoding within sensorimotor cortex has been well established (22). We therefore postulated that in normal-appearing cortex, differences in the representations of monosyllabic and polysyllabic words would be apparent in the neural signals restricted to the lateral primary motor area (M1). We separated trials in which participants vocalized monosyllabic words from those in which they vocalized polysyllabic words (Fig. 4*A*). In normal-appearing cortex, we found greater mean high-gamma activity during polysyllabic trials (460 to 520 ms, $P < 0.05$; Bonferroni-corrected) when compared to monosyllabic trials. Linear mixed-effects modeling confirmed that mean high-gamma activity during vocalization of polysyllabic words was significantly higher than that during vocalization of monosyllabic words. However, in glioma-infiltrated cortex, differences between polysyllabic and monosyllabic trial conditions were not apparent.

Because neurons primarily operate in a multivariate environment (23), any circuit-level analysis that does not utilize multivariate models would be incomplete. For instance, a lack of difference on univariate analysis between two signals does not guarantee that the circuit maintains the same representation for the two trial conditions. Therefore, we confirmed the apparent differences in computational properties of normal-appearing and glioma-infiltrated cortex by evaluating the decodability of their signals using multivariate models. We first trained a Bernoulli Naıve Bayes classifier to distinguish between monosyllabic and polysyllabic trial conditions using event-related responses (Fig. 4*B*). We implemented identical training and cross-validation paradigms (i.e., leave-one-subject-out-cross-validation) for both conditions. As expected, normal-appearing cortex produced above-chance decoding between monosyllabic and polysyllabic trials (mean classifier accuracy = 0.569, $P < 0.001$). By contrast, in glioma-infiltrated cortex, we were not able to decode monosyllabic from polysyllabic trials above chance (mean classifier accuracy = 0.516, $P = 0.330$). This pattern was maintained for support vector machine and artificial neural network decoders (*SI Appendix*, Fig. S5). Linear mixed-effects modeling confirmed that decoding accuracies were significantly higher in normal-appearing cortex compared to glioma-infiltrated cortex ($P = 0.019$). This effect persisted in the subgroup of participants with noncodeleted gliomas ($P = 0.020$). No differences in decoding accuracies were found between participants with codeleted and nonco-deleted gliomas ($P = 0.294$).

Discussion

Emerging developments into the cellular- and network-level electrophysiologic interactions between neurons and gliomas raise critical questions about how altered neuronal circuits represent and encode information in humans. Astrocytic gliomas form interconnected networks (8) that substantially modulate the excitability of neurons (11) through paracrine signaling and synaptogenesis (3, 24). Oligodendrogliomas are similarly associated with increased cortical excitability, though likely via different mechanisms (13). Therefore, the consequences of glioma infiltration for neuronal processing could range anywhere from the loss of event-related synchronicity to the relative preservation of circuit dynamics. Here, we show that glioma-infiltrated cortex retains the ability to engage in coordinated neural responses during the planning and production of speech but has a diminished entropy which may stem from glioma synaptic signaling that biases the activity of these networks at baseline (11). Furthermore, salient features of a given cognitive/behavioral event (in this case, vocalization of mono- versus polysyllabic words) could not be temporally decoded from its neural signals. Glioma-infiltrated cortex additionally demonstrates a broad spatial distribution of activity during speech. This prompts an exploration of how neuron-glioma communication contributes to reduced functional states and highlights the need for more targeted analysis of neuromodulation in patients with malignant gliomas.

We arrived at these findings by first demonstrating via subdural ECoG that glioma-infiltrated cortex is capable of synchronizing its activity to the onset of speech. This is in line with evidence from the neurosurgical literature where functional cortex in regions of glioma infiltration has been described during brain mapping, which was redemonstrated here (*SI Appendix*, Fig. S3) in overlapping speech areas (25, 26). For instance, evoked magnetic responses have been shown in glioma-infiltrated sensorimotor cortex after tactile stimulation (27), motor and language function can be transiently inhibited and localized via direct electrical stimulation of glioma-infiltrated cortex (28, 29), and resection of glioma-infiltrated regions with high functional connectivity to the rest of the brain leads to permanent neurological injury (30, 31). However, the spatiotemporal dynamics underlying these phenomena have, up until now, remained largely unexplored. These findings directly demonstrate that glioma-infiltrated cortex participates in coordinated neural responses during speech production while maintaining that its spatial and temporal patterns of activity are indeed distinct from normal-appearing cortex.

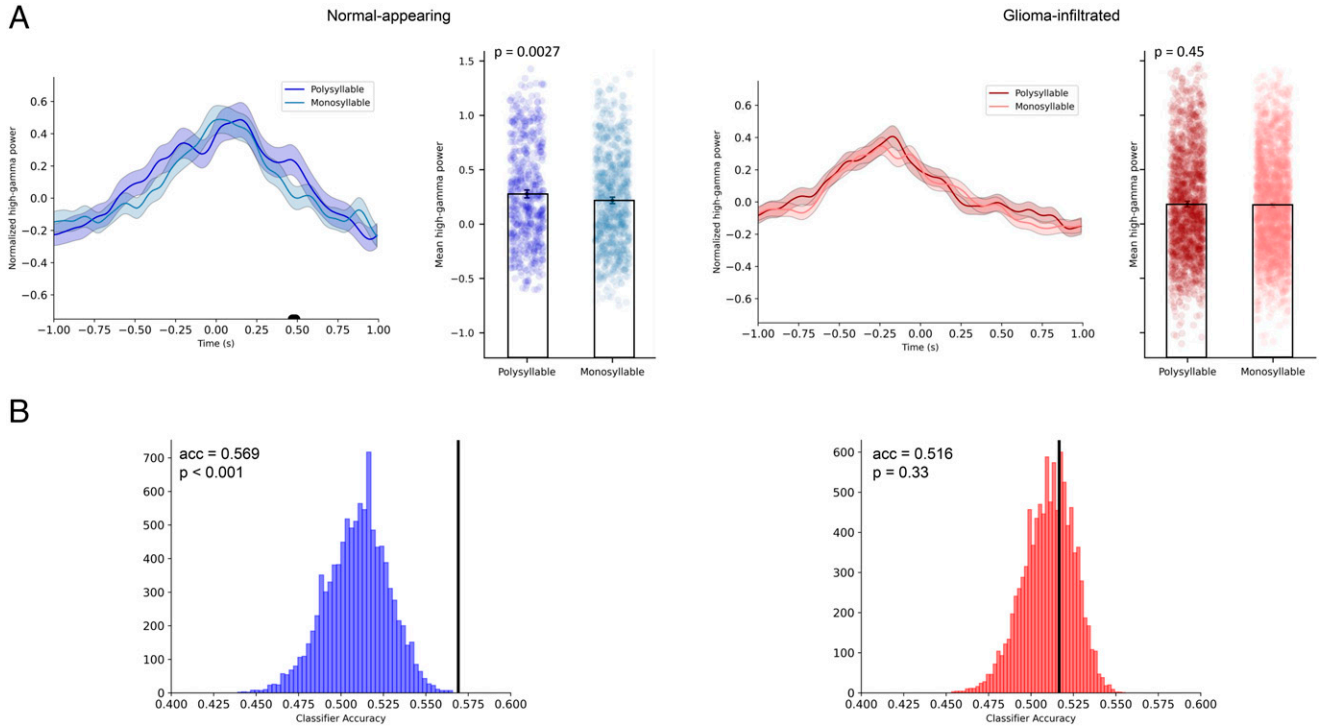

Fig. 4. Decodability of signals from normal-appearing and glioma-infiltrated cortex in motor areas. (*A*) In normal-appearing cortex, ERSPs during vocalization of polysyllabic words demonstrate unique temporal features. Using linear mixed-effects modeling, mean high-gamma activity in normal-appearing cortex was found to be significantly higher during vocalization of polysyllabic words ($P = 0.0027$). In glioma-infiltrated cortex, no statistically significant differences in high-gamma activity were found between polysyllabic and monosyllabic trial conditions. Black bar indicates time points in which the *t* test *P* value exceeded a threshold of $P < 0.05$ after Bonferroni corrections. (*B*) Above-chance decoding of monosyllabic from polysyllabic trials was achieved across in normal-appearing cortex (*Left*) but not in glioma-infiltrated cortex (*Right*) using a Bernoulli Naïve Bayes classifier. Decoding accuracy (acc; black bars) was significantly higher in normal-appearing cortex compared to glioma-infiltrated cortex ($P = 0.019$).

This is especially apparent from the comparative spatial distributions of high-gamma activity in normal-appearing and glioma-infiltrated cortex. Under physiologic conditions, prespeech activity during visual confrontation naming localizes to a well-defined circuit, including the pars orbitalis and pars triangularis of the inferior frontal gyrus where semantic-to-lexical mapping takes place (32, 33). Here, we show that normal-appearing cortex roughly adheres to this canonical network as the regions of maximal high-gamma activity were centered on the rostral inferior frontal gyrus. Conversely, we found that glioma-infiltrated cortex recruited a diffuse network of atypical cortical regions during speech planning, including caudal portions of the middle frontal gyrus. Parallel reports of cortical redistribution of language function to atypical peritumoral sites, including the middle frontal gyrus, have been reported with PET (34, 35) and fMRI (36) but chiefly attributed the phenomenon to physiologic neuroplasticity (26, 37). In the context of the present study and evidence of coordinated high-gamma responses in glioma-infiltrated cortex, the widespread recruitment of perisylvian cortex in such regions may reflect activation of the inherently diffuse, interconnected neuron-to-glioma network, though this mechanism may vary based on the glioma subtype (38). Therefore, it is unclear whether the increased spatial representation acts as a short-range mechanism of native compensation for the loss of temporally encoded information in glioma-infiltrated cortex or is simply a pathologic signature of glioma infiltration. Further work in nonhuman disease models will be required to determine the temporal evolution of these interacting electrophysiologic and oncologic processes.

The next critical question in light of this evidence is if glioma-infiltrated cortex can generate robust synchronous activity during speech in a manner similar to normal-appearing cortex, why do patients with infiltrative gliomas often present with aphasia (i.e., speech impairment)? Prior accounts of the pathophysiology of aphasia in patients with glioma have mainly focused on disruptions in anatomic and functional connectivity involving the perisylvian language network (10, 39). Here, we provide a more mechanistic account by demonstrating that the neuronal subpopulations within glioma-infiltrated cortex have inherently lower entropies, as demonstrated by their diminished response variability across time (Fig. 3 *A* and *B*), which may stem from glioma synaptic signaling that biases the activity of these networks at baseline (11). Indeed, the diminished entropy of glioma-infiltrated cortex (a proxy for information-encoding capacity), even in nonaphasic patients, may be indicative of alterations in cognitive processing that, when further deteriorated, may lead to aphasia.

To further interrogate whether nuanced aspects of speech processing are altered in glioma-infiltrated cortex, we applied a stepwise procedure starting with a simple univariate model and progressing to more complex multivariate models (i.e., Artificial Neural Networks [ANNs]). In normal-appearing cortex, we demonstrated a difference on univariate analysis, which implies that bursts of high-gamma activity may be part of the circuit's encoding strategy during speech production. Such differences were not observed in glioma-infiltrated cortex. The decoding of speech via ECoG is notoriously difficult without the use of highly expressive multivariate models such as ANNs (40, 41). Here, we implement three distinct multivariate models to

ultimately demonstrate that glioma-infiltrated cortex processes information in a manner that is fundamentally different from normal-appearing cortex.

By providing a model for network-level electrophysiologic alterations in glioma-infiltrated cortex, our data carry important considerations for therapeutic avenues such as neuroprostheses and neuromodulation. In terms of neuroprostheses, prior work was limited to participants with intact speech and cortical function, and therefore the applicability to clinical populations has been debated. However, in a recent landmark study by Moses et al., a neuroprosthesis capable of decoding speech was successfully implanted in an anarthric patient who suffered from a brainstem stroke over a decade prior (42). Because it was unknown whether the patient's cortex was still capable of producing decodable neural representations of speech after years of disuse and ensuing plasticity, the results provided a compelling basis for clinical translation to patients with chronic speech impairments.

Whether similar results could be achieved in patients with aphasia is unknown. This is especially salient considering many low-grade gliomas are now considered chronic illnesses (slowly evolving over decades), thereby increasing the prevalence of aphasia (and other potentially targetable neurological impairments) in this population. To determine whether neuroprostheses are feasible in gliomas, it is first necessary to establish the computational landscape of both apparently normal and tumor-infiltrated cortex. Here, we show that regions of the cortex infiltrated by malignant glioma are not electrically silent. Indeed, they synchronize their activity to speech events, though with decreased statistical variability (i.e., entropy) and ability to encode nuanced articulatory trajectories, which may complicate but not preclude neural decoding. Considering functionally relevant glioma-infiltrated cortex is left intact during cancer directed therapies such as resective surgery, it is conceivable that a neuroprosthesis could encompass areas of glioma-infiltrated brain. We provide evidence that because a greater area of the cortex is recruited when infiltrated by glioma (whether this is compensatory or pathologic remains unknown), a successful prosthesis may need to span regions of cortex that are not traditionally implicated in speech processing.

Neuromodulation presents an equally intriguing therapeutic avenue for gliomas. However, to date, there have been no clinical trials investigating the use of neuromodulation in gliomas despite compelling evidence that excitatory synaptic input onto gliomas promotes tumor invasion. In principle, it may be possible to apply neuromodulation to attenuate the abnormal excitation found within glioma-infiltrated cortex and slow the progression of disease (6). The present study invokes an additional layer of complexity to the use of neuromodulation in glioma: because glioma-infiltrated cortex demonstrates synchronized activity during speech production, modulating these circuits may have implications for cognition/behavior as well. Whether neuromodulation could be exploited to simultaneously inhibit glioma proliferation and improve functional processing is unknown and requires further investigation.

Limitations. Our work presents several limitations. First, while Shannon entropy provides a useful method for quantifying the statistical variability of signals, and therefore insight into how a system processes information, it is only a proxy for information-encoding capacity. For instance, systems with relatively low entropy may still be able to faithfully encode information, albeit with lower efficiencies than ones with high entropy. Second, the analyses presented are restricted to the high-gamma range. Cortical high-gamma signal has been used extensively to interrogate speech processing in humans. We acknowledge that the association between high-gamma activity and neuronal activity is not straightforward in humans (43). Further work is required to develop a greater understanding of this relationship, especially in the setting of malignant gliomas, and the significance of other frequency bands. Third, this work is cross-sectional in nature and therefore cannot capture the evolving impact of treatment and disease progression on cortical processing. Finally, several distinct glioma subtypes (i.e., IDH-mutant 1p/19 codeleted oligodendrogliomas and astrocytic gliomas) were investigated. While each glioma subtype may simply exploit a different mechanism to arrive at the overall phenotype identified in our manuscript, future studies are required to delineate the evolution of this process and determine whether tumor molecular biology affects local neural circuitry in a more nuanced manner.

Materials and Methods

Participant Characteristics and Experimental Workflow. To assess the computational capacity of glioma-infiltrated cortex with respect to language, invasive electrophysiologic recordings were taken from 12 adult patients with perisylvian gliomas on the surface of the brain while they engaged in a visual confrontation naming (i.e., picture naming) task during awake craniotomy. All participants provided written informed consent to participate in this study, which was approved by the institutional review board (CHR-17-23215) at the University of California San Francisco and performed in accordance with the Declaration of Helsinki.

Participant demographics and final pathologic diagnoses are presented in *SI Appendix*, Table S1. The hemisphere of language dominance was determined using baseline magnetic source imaging (14, 15). Briefly, our participants sat in a 275-channel whole-head CTF Omega 2000 system (CTF Systems, Inc.) sampling at 1,200 Hz while they performed an auditory-verb generation task. The resulting time series were then reconstructed in source space with an adaptive spatial filter after registration with high-resolution MRI. Finally, changes in beta-band activity during verb generation were compared across hemispheres to generate an overall laterality index. All 12 participants were left-dominant and underwent electrophysiologic recording of the left hemisphere. Final pathologic diagnoses incorporating tumor molecular characteristics were updated in accordance with the 2021 World Health Organization Classification of Tumors of the Central Nervous System (44). Mutation status at IDH-1 and IDH-2 loci was determined via immunohistochemistry; 1p-19q codeletion was determined via fluorescence in situ hybridization.

We implemented an intraoperative testing paradigm previously established in refs. 45 and 46. Noise in the operating room was minimized through rigorous enforcement of the following: 1) all personnel were requested to cease verbal communication, 2) telephones and alarms were muted, and 3) surgical suction and all other nonessential machinery were temporarily shut down. A 15-inch laptop computer (60 Hz refresh rate) running a custom MATLAB script integrated with PsychToolbox 3 (http://psychtoolbox.org/) was placed 30 cm away from each participant. The script initiated a picture naming task that consisted of a single block of 48 unique stimuli, each depicting a common object or animal via colored line drawings. Each stimulus was presented at the point of central fixation and occupied 75% of the display. Upon presentation of each stimulus, participants were required to vocalize a single word that best described the item. Twenty-eight of the correct speech responses were monosyllabic words while 20 were polysyllabic. The stimuli were manually advanced by the clinician either a) immediately after a verbal response was given or b) after 6 s if no verbal response was given. A trigger was sent to the biosignal acquisition device (g.tec) at the onset of each new stimulus to enable calculation of the speech latency.

Each participant received a training session 2 d prior to participation to ensure familiarity with the task and underwent 1) a minimum anesthesia washout period of 20 min and 2) an extensive postemergence wakefulness assessment to ensure adequate arousal during intraoperative language testing (45).

Signal Acquisition and Preprocessing. To extract local cortical responses during a speech event of interest (i.e., vocalization of a monosyllabic word), participants underwent simultaneous audio and electrophysiologic recordings. Audio was sampled at 44.1 kHz from a dual-channel microphone placed 5 cm from the participant and electrophysiologic signals were amplified (g.tec) and sampled at 4,800 Hz from multichannel low-density (20 electrodes, 10 mm spacing) and high-density (96 electrodes, 3 mm spacing) platinum subdural electrocorticography grids (Ad-Tech). During offline analyses, audio and electrophysiologic recordings were manually aligned, resampled, and segmented into epochs (speech-locked). These epochs set time = 0 ms as speech onset and

included ± 2,000 ms for a total of 4,000 ms of signal per trial. Trials were discarded if a) an incorrect response was given (including fillers and interjections) or b) there was a >2 s delay between stimulus presentation and response so as to maintain consistent trial dynamics and ensure that the neural signal indeed reflected the experimental manipulations (*SI Appendix*, Table S2). Noisy channels were automatically rejected if their kurtosis exceeded 5.0. Electrodes were subsequently rereferenced to the common average for each participant.

Because transient increases in high-gamma power are strongly correlated with the spiking activity of local ensembles and thus reflect fundamental units of neural computation (47, 48), we focused our subsequent analyses on ERSPs in the high-gamma range. To extract the ERSPs, electrophysiologic signals were first down-sampled to 600 Hz, then high-pass filtered at 0.1 Hz to remove DC-offset and low frequency drift, notch filtered at 60 Hz and its harmonics to remove line noise, and bandpass filtered between 70 and 170 Hz (i.e., the high-gamma range) using a Hamming windowed sinc FIR filter. Spectral power was extracted as the squared magnitude of the analytic signal, calculated using the Hilbert transform (49). These signals were finally smoothed using a 100 ms Gaussian kernel, down-sampled to 100 Hz, and z-scored across each trial. All signal preprocessing was conducted using EEGLAB (50) (version 2021.0; https://sccn.ucsd.edu/eeglab/index.php).

Grid Localization and Identification of Glioma-Infiltrated Cortex. To determine whether a given electrophysiologic signal originated from glioma-infiltrated or normal-appearing cortex, the subdural electrocorticography grids were localized via a combination of intraoperative photography and stereotactic techniques (51, 52). For each participant, intraoperative photographs of the cortex taken with and without the grid(s) were used to register the grids to reconstructions of the pial surface and vascular anatomy and extract the three-dimensional coordinate of each electrode. Each electrode coordinate was then registered to the T2-weighted FLAIR image and labeled as "glioma-infiltrated" or "normal-appearing" by a trained coauthor blinded to the electrophysiologic data (11). Glioma-infiltrated regions were defined based on two criteria previously established in the literature (53): 1) a confluent and mass-like area of abnormally elevated signal on T2-weighted FLAIR sequences and 2) a lack of contrast enhancement on T1-postgadolinium sequences. Imaging was confirmed with gross inspection of the cortex confirming dilation and/or an abnormal vascular pattern. Prior work has shown that these regions of "nonenhancing" disease consist of infiltrating tumor cells intermixed with neurons and normal glial cells. Furthermore, it is precisely these regions that demonstrate altered excitability and potentially cortical processing (1, 11). These labels were reviewed by a study principal investigator (S.L.H.-J.) and compared to labels derived during intraoperative stereotactic neuro-navigation to reach a consensus (Brainlab). Finally, electrode coordinates were registered to a common surface (MNI template) for each participant to facilitate group comparisons and regions of interest were defined according to the Automated Anatomical Labeling atlas (54) (https://www.gin.cnrs.fr/en/tools/aal/). Enantiomorphic normalization was used to account for brain shift due to edema or tumor mass effect. Image registration and normalization routines were conducted using SPM12 (https://www.fil.ion.ucl.ac.uk/spm/software/spm12/) and ANTsR (version 0.40; https://github.com/ANTsX/ANTsR) and surface reconstruction using FreeSurfer (55) (version 7.1; https://surfer.nmr.mgh.harvard.edu/). The location of grid implantation was solely directed by clinical indications. For each participant, accuracy of the final registration was independently confirmed by a research technician and a board-certified neurosurgeon. Specifically, gyral and sulcal anatomy was used to triangulate the location of each electrode registered to the template surface and was then compared to intraoperative photographs of the actual cortex with the overlying grid(s), a highly accurate method for cortical grid registration (56). Individual grid trajectories for each participant are presented in *SI Appendix*, Fig. S2.

Language Mapping. To determine the functional relevance of glioma-infiltrated cortex, awake language mapping with direct electrical stimulation was implemented in all 12 participants according to previously established protocols (19, 20, 29). Briefly, for each square centimeter of exposed cortex, bipolar stimulation (60 Hz, 1.5 to 6 mA) was applied 1.4 s prior to the onset of a picture naming stimulus. If stimulation of a given site led to one of several language errors (anomia, semantic/phonological paraphasia, circumlocution, or neologism) on two out of three stimulation trials, that site was considered a "positive" language site. After-discharge potentials were monitored via electrocorticography; iced Ringer's lactate and Propofol were readily available. Positive stimulation sites were manually registered with known cortical grid trajectories via intraoperative photography and localized on the common cortical surface.

Information Theoretical Analysis. Shannon entropy was used as a statistical proxy for the relative capacity of glioma-infiltrated cortex to encode task-relevant information compared to normal-appearing cortex. In general, systems with high entropy demonstrate substantial variability across trial conditions and are thus capable of encoding more information than those with low entropy (21, 57). Two methods were used to measure the entropy of signals originating from normal-appearing and glioma-infiltrated cortex. First, Shannon entropy was computed at each time point in the ERSPs simultaneously across all trial conditions to extract time courses of encoding capacity of normal-appearing and glioma-infiltrated cortex (Neuroscience Information Theory Toolbox, https://github.com/nmtimme/Neuroscience-Information-Theory-Toolbox) (58). Next, the Shannon entropy was calculated separately for each trial to derive estimates of overall response variability of normal-appearing and glioma-infiltrated cortex by discretizing each ERSP into probability mass functions consisting of 10 equally spaced bins (7) (Scipy, version 1.6.1; https://www.scipy.org/).

Neural Decoding. Finally, the decodability of signals arising from normal-appearing and glioma-infiltrated cortex was determined by training classifiers to distinguish between monosyllabic and polysyllabic trials across all participants. For this analysis, only electrodes from motor cortex were selected, as they are most relevant to predictability of articulation. It should be noted that not all participants presented with both glioma-infiltrated and normal-appearing electrodes over motor cortex, so this analysis is comprised of 10 rather than 12 participants (*SI Appendix*, Table S2). Glioma-infiltrated and normal-appearing electrodes were separated into two groups, and the following steps were repeated exactly the same for both groups. Features were composed of electrode-level time series of individual trials, and targets were encoded as a binary label of trial-type (1 for monosyllabic, 0 for polysyllabic). Given its prior use to quantify information encoding in neural populations and its parallels to the Shannon entropy method, a Bernoulli Naïve Bayes (alpha = 1.0) classifier was presented for the primary analyses (59). Two additional classifiers were trained and tested given their ability to fit increasingly complex relationships between the features: support vector machine (RBF kernel, L2-penalty, C = 0.5), and an ANN with one hidden layer (256 hidden units), ReLU activation, and an L2-penalty of $5*10^{-4}$. The ANN was trained using an Adam optimizer with initial learning rate 1×10^{-3}, batch size 64 (shuffled on each iteration), and early stopping after 20 iterations with no loss improvement on a held-out 10% validation set.

The train-test split for each classifier was established using a leave-one-subject-out-cross-validation approach, such that each classifier was trained on the data from all participants except for one and was used to predict the trials of that left-out subject. This was performed across all subject-folds and classifier predictions were aggregated across participants. Confusion matrices were calculated using this aggregated participant data, and accuracy was calculated as the ratio of the trace of the confusion matrix to the sum of all its entries. Accuracy was evaluated for statistical significance using a nonparametric permutation test. This process was repeated (n = 10,000) using shuffled target labels in order to establish a null distribution, and test accuracy was assessed for significance against this distribution. Decoding accuracies were compared between normal-appearing and glioma-infiltrated cortex via linear mixed-effects modeling with the pair of accuracies from each participant serving as the repeated measure. This method was used to generate an estimate of the effect including participants without a full pair of data points (*SI Appendix*, Table S2).

Data Visualization and Statistical Analysis. Template cortical surface visualization was performed via FieldTrip (60) (https://github.com/fieldtrip/fieldtrip) and lesion overlap maps were generated using svrlsmgui (61) (https://github.com/atdemarco/svrlsmgui). Linear mixed-effects modeling was used to perform statistical comparisons with repeated measures via the nlme package in R (https://cran.r-project.org/web/packages/nlme/citation.html). The signal's origin (i.e., normal-appearing/glioma-infiltrated cortex) was modeled as a fixed effect and the participants were modeled as random effects. Significance between contrast estimates were calculated using the multcomp package in R (https://cran.r-project.org/web/packages/multcomp/index.html). For continuous variables without repeated measures, t tests were used. A threshold of $P < 0.05$ was used to denote statistical significance and corrections for multiple comparisons were made using the Bonferroni method.

Data Availability. The data that support the findings of this study are available on request from the corresponding authors. The data are not publicly available because they could compromise research participant

privacy and consent. All original code has been deposited at Zenodo (https://doi.org/10.5281/zenodo.5604530) and is publicly available as of the date of publication. Any additional information required to reanalyze the data reported in this paper is available from the corresponding authors upon request.

ACKNOWLEDGMENTS This study was supported by the NIH grants K08NS110919 and P50CA097257, the Robert Wood Johnson Foundation grant 74259, the UCSF LoGlio Collective, the Sheri Sobrato Brisson Brain Cancer Fund to S.L.H.-J., the Sullivan Brain Cancer Fund to S.K., and the NIH grant R00DC013828 to D.B.

1. S. Krishna *et al.*, Glioblastoma remodeling of neural circuits in the human brain decreases survival. bioRxiv [Preprint] (2021). https://doi.org/10.1101/2021.02.18.431915 (Accessed 1 May 2021).
2. V. Venkataramani *et al.*, Glutamatergic synaptic input to glioma cells drives brain tumour progression. *Nature* **573**, 532–538 (2019).
3. H. S. Venkatesh *et al.*, Neuronal activity promotes glioma growth through neuroligin-3 secretion. *Cell* **161**, 803–816 (2015).
4. A. G. S. Daniel *et al.*, Functional connectivity within glioblastoma impacts overall survival. *Neuro-oncol.* **23**, 412–421 (2020).
5. P. Fries, Rhythms for cognition: Communication through coherence. *Neuron* **88**, 220–235 (2015).
6. G. Sprugnoli, A. J. Golby, E. Santarnecchi, Newly discovered neuron-to-glioma communication: New noninvasive therapeutic opportunities on the horizon? *Neuro-oncol. Adv.* **3**, vdab018 (2021).
7. R. Quian Quiroga, S. Panzeri, Extracting information from neuronal populations: Information theory and decoding approaches. *Nat. Rev. Neurosci.* **10**, 173–185 (2009).
8. M. Osswald *et al.*, Brain tumour cells interconnect to a functional and resistant network. *Nature* **528**, 93–98 (2015).
9. E. Jung *et al.*, Tweety-homolog 1 drives brain colonization of gliomas. *J. Neurosci.* **37**, 6837–6850 (2017).
10. B. Yuan *et al.*, Resting-state functional connectivity predicts individual language impairment of patients with left hemispheric gliomas involving language network. *Neuroimage Clin.* **24**, 102023 (2019).
11. H. S. Venkatesh *et al.*, Electrical and synaptic integration of glioma into neural circuits. *Nature* **573**, 539–545 (2019).
12. S. L. Campbell, S. C. Buckingham, H. Sontheimer, Human glioma cells induce hyperexcitability in cortical networks. *Epilepsia* **53**, 1360–1370 (2012).
13. H. Chen *et al.*, Mutant IDH1 and seizures in patients with glioma. *Neurology* **88**, 1805–1813 (2017).
14. R. C. Doss, W. Zhang, G. L. Risse, D. L. Dickens, Lateralizing language with magnetic source imaging: Validation based on the Wada test. *Epilepsia* **50**, 2242–2248 (2009).
15. A. M. Findlay *et al.*, Dynamics of hemispheric dominance for language assessed by magnetoencephalographic imaging. *Ann. Neurol.* **71**, 668–686 (2012).
16. A. A. Aabedi *et al.*, Convergence of heteromodal lexical retrieval in the lateral prefrontal cortex. *Sci. Rep.* **11**, 6305 (2021).
17. A. Flinker *et al.*, Redefining the role of Broca's area in speech. *Proc. Natl. Acad. Sci. U.S.A.* **112**, 2871–2875 (2015).
18. K. J. Forseth *et al.*, A lexical semantic hub for heteromodal naming in middle fusiform gyrus. *Brain* **141**, 2112–2126 (2018).
19. R. A. Morshed, J. S. Young, A. T. Lee, M. S. Berger, S. L. Hervey-Jumper, Clinical pearls and methods for intraoperative awake language mapping. *Neurosurgery* **89**, 143–153 (2020).
20. S. L. Hervey-Jumper *et al.*, Awake craniotomy to maximize glioma resection: Methods and technical nuances over a 27-year period. *J. Neurosurg.* **123**, 325–339 (2015).
21. R. A. A. Ince, R. S. Petersen, D. C. Swan, S. Panzeri, Python for information theoretic analysis of neural data. *Front. Neuroinform.* **3**, 4 (2009).
22. J. Chartier, G. K. Anumanchipalli, K. Johnson, E. F. Chang, Encoding of articulatory kinematic trajectories in human speech sensorimotor cortex. *Neuron* **98**, 1042–1054.e4 (2018).
23. D. Beniaguev, I. Segev, M. London, Single cortical neurons as deep artificial neural networks. *Neuron* **109**, 2727–2739.e3 (2021).
24. C. C. John Lin *et al.*, Identification of diverse astrocyte populations and their malignant analogs. *Nat. Neurosci.* **20**, 396–405 (2017).
25. P. C. De Witt Hamer, S. G. Robles, A. H. Zwinderman, H. Duffau, M. S. Berger, Impact of intraoperative stimulation brain mapping on glioma surgery outcome: A meta-analysis. *J. Clin. Oncol.* **30**, 2559–2565 (2012).
26. H. Duffau, Lessons from brain mapping in surgery for low-grade glioma: Insights into associations between tumour and brain plasticity. *Lancet Neurol.* **4**, 476–486 (2005).
27. H. Schiffbauer, P. Ferrari, H. A. Rowley, M. S. Berger, T. P. Roberts, Functional activity within brain tumors: A magnetic source imaging study. *Neurosurgery* **49**, 1313–1320, discussion 1320–1321 (2001).
28. E. F. Chang *et al.*, Functional mapping-guided resection of low-grade gliomas in eloquent areas of the brain: Improvement of long-term survival. Clinical article. *J. Neurosurg.* **114**, 566–573 (2011).
29. N. Sanai, Z. Mirzadeh, M. S. Berger, Functional outcome after language mapping for glioma resection. *N. Engl. J. Med.* **358**, 18–27 (2008).
30. A. T. Lee *et al.*, The impact of high functional connectivity network hub resection on language task performance in adult low- and high-grade glioma. *J. Neurosurg.* **134**, 1102–1112 (2020).
31. P. E. Tarapore *et al.*, Magnetoencephalographic imaging of resting-state functional connectivity predicts postsurgical neurological outcome in brain gliomas. *Neurosurgery* **71**, 1012–1022 (2012).
32. Y. Hoshi *et al.*, Spatiotemporal characteristics of hemodynamic changes in the human lateral prefrontal cortex during working memory tasks. *Neuroimage* **20**, 1493–1504 (2003).
33. N. De Pisapia, J. A. Slomski, T. S. Braver, Functional specializations in lateral prefrontal cortex associated with the integration and segregation of information in working memory. *Cereb. Cortex* **17**, 993–1006 (2007).
34. P. T. Meyer *et al.*, Preoperative mapping of cortical language areas in adult brain tumour patients using PET and individual non-normalised SPM analyses. *Eur. J. Nucl. Med. Mol. Imaging* **30**, 951–960 (2003).
35. A. Thiel *et al.*, Plasticity of language networks in patients with brain tumors: A positron emission tomography activation study. *Ann. Neurol.* **50**, 620–629 (2001).
36. H. Duffau, L. Bauchet, S. Lehéricy, L. Capelle, Functional compensation of the left dominant insula for language. *Neuroreport* **12**, 2159–2163 (2001).
37. M. Desmurget, F. Bonnetblanc, H. Duffau, Contrasting acute and slow-growing lesions: A new door to brain plasticity. *Brain* **130**, 898–914 (2007).
38. S. Krishna, S. Kakaizada, N. Almeida, D. Brang, S. Hervey-Jumper, Central nervous system plasticity influences language and cognitive recovery in adult glioma. *Neurosurgery* **89**, 539–548 (2021).
39. A. Bizzi *et al.*, Aphasia induced by gliomas growing in the ventrolateral frontal region: Assessment with diffusion MR tractography, functional MR imaging and neuropsychology. *Cortex* **48**, 255–272 (2012).
40. J. G. Makin, D. A. Moses, E. F. Chang, Machine translation of cortical activity to text with an encoder-decoder framework. *Nat. Neurosci.* **23**, 575–582 (2020).
41. D. A. Moses, M. K. Leonard, J. G. Makin, E. F. Chang, Real-time decoding of question-and-answer speech dialogue using human cortical activity. *Nat. Commun.* **10**, 3096 (2019).
42. D. A. Moses *et al.*, Neuroprosthesis for decoding speech in a paralyzed person with anarthria. *N. Engl. J. Med.* **385**, 217–227 (2021).
43. J. R. Manning, J. Jacobs, I. Fried, M. J. Kahana, Broadband shifts in local field potential power spectra are correlated with single-neuron spiking in humans. *J. Neurosci.* **29**, 13613–13620 (2009).
44. D. N. Louis *et al.*, The 2021 WHO classification of tumors of the central nervous system: A summary. *Neuro-oncol.* **23**, 1231–1251 (2021).
45. A. A. Aabedi *et al.*, Assessment of wakefulness during awake craniotomy to predict intraoperative language performance. *J. Neurosurg.* **132**, 1930–1937 (2019).
46. A. A. Aabedi *et al.*, Balancing task sensitivity with reliability for multimodal language assessments. *J. Neurosurg.* **1**, 1–8 (2021).
47. S. Ray, N. E. Crone, E. Niebur, P. J. Franaszczuk, S. S. Hsiao, Neural correlates of high-gamma oscillations (60-200 Hz) in macaque local field potentials and their potential implications in electrocorticography. *J. Neurosci.* **28**, 11526–11536 (2008).
48. G. Buzsáki, X.-J. Wang, Mechanisms of gamma oscillations. *Annu. Rev. Neurosci.* **35**, 203–225 (2012).
49. https://doi.org/10.5281/zenodo.5604530.
50. A. Delorme, S. Makeig, EEGLAB: An open source toolbox for analysis of single-trial EEG dynamics including independent component analysis. *J. Neurosci. Methods* **134**, 9–21 (2004).
51. S. S. Dalal *et al.*, Localization of neurosurgically implanted electrodes via photograph-MRI-radiograph coregistration. *J. Neurosci. Methods* **174**, 106–115 (2008).
52. D. Gupta, N. J. Hill, M. A. Adamo, A. Ritaccio, G. Schalk, Localizing ECoG electrodes on the cortical anatomy without post-implantation imaging. *Neuroimage Clin.* **6**, 64–76 (2014).
53. J. E. Villanueva-Meyer, M. C. Mabray, S. Cha, Current clinical brain tumor imaging. *Neurosurgery* **81**, 397–415 (2017).
54. E. T. Rolls, C.-C. Huang, C.-P. Lin, J. Feng, M. Joliot, Automated anatomical labelling atlas 3. *Neuroimage* **206**, 116189 (2020).
55. A. M. Dale, B. Fischl, M. I. Sereno, Cortical surface-based analysis. I. Segmentation and surface reconstruction. *Neuroimage* **9**, 179–194 (1999).
56. T. A. Pieters, C. R. Conner, N. Tandon, Recursive grid partitioning on a cortical surface model: An optimized technique for the localization of implanted subdural electrodes. *J. Neurosurg.* **118**, 1086–1097 (2013).
57. A. Borst, F. E. Theunissen, Information theory and neural coding. *Nat. Neurosci.* **2**, 947–957 (1999).
58. N. M. Timme, C. Lapish, A tutorial for information theory in neuroscience. *eNeuro* **5**, ENEURO.0052-18.2018 (2018).
59. A. Pouget, P. Dayan, R. Zemel, Information processing with population codes. *Nat. Rev. Neurosci.* **1**, 125–132 (2000).
60. R. Oostenveld, P. Fries, E. Maris, J.-M. Schoffelen, FieldTrip: Open source software for advanced analysis of MEG, EEG, and invasive electrophysiological data. *Comput. Intell. Neurosci.* **2011**, 156869 (2011).
61. A. T. DeMarco, P. E. Turkeltaub, A multivariate lesion symptom mapping toolbox and examination of lesion-volume biases and correction methods in lesion-symptom mapping. *Hum. Brain Mapp.* **39**, 4169–4182 (2018).